ADANA ALPARSLAN TÜRKEŞ BİLİM VE TEKNOLOJİ ÜNİVERSİTESİ BİLİM DERGİSİ
ADANA ALPARSLAN TÜRKEŞ SCIENCE AND TECHNOLOGY UNİVERSITY JOURNAL OF SCIENCE
Research Article www.dergipark.com/atujscience

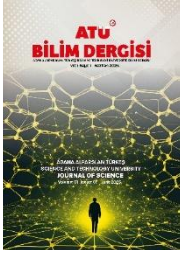

A strategy for enhancing the performance of CdS-based hybrid photovoltaic cells via Co addition

Salih Yılmaz[1,#], Murat Tomakin[2], Emin Bacaksız[3]

[1]Adana Alparslan Türkeş Science and Technology University, Department of Materials Science and Engineering, 01250 Adana, Türkiye

ORCID: 0000-0002-3006-4473

[2]Recep Tayyip Erdoğan University, Department of Physics, 53100 Rize, Türkiye

ORCID: 0000-0003-1887-848X

[3]Karadeniz Technical University, Department of Physics, 61080 Trabzon, Türkiye

ORCID: 0000-0002-0041-273X

#Corresponding Author:

E-mail: salihyilmaz@atu.edu.tr

Abstract

This paper demonstrates the positive role of Co atoms on the performance of CdS-based hybrid photovoltaics. Spherical shaped CdS and CdS:Co films were grown on indium tin oxide (ITO)-covered glass slides, while P3HT was individually covered on these spheres. The transparency of devices improved with introducing the Co atoms into CdS matrix in the near infrared region, while a corresponding reduction in absorption was noted. Photoluminescence (PL) data showed that a diminish in the peak intensity of PL, suggesting the development of additional defect levels in the band gap which behaves as non-radiative recombination centers. The current density-voltage (J-V) characteristics indicated that the ITO/N719/CdS:Co(5%)/P3HT/Ag device achieved an overall efficiency of 0.028%, representing almost a sixfold increase over the control device. This enhancement is possibly attributed to the enhanced generation of electron-hole pairs owing to effective charge separation at the CdS:Co/P3HT interface.

Keywords: CdS:Co thin films; P3HT; CBD; optical properties; power conversion efficiency

CdS tabanlı hibrit fotovoltaik hücrelerin performansını Co ekleme yoluyla iyileştirmeye yönelik bir strateji

Öz

Bu makale, CdS tabanlı hibrit güneş hücrelerinin performansında Co atomlarının olumlu rolünü ortaya koymaktadır. Küresel şekilli CdS ve CdS:Co filmler indiyum kalay oksit (ITO) kaplı cam plakalar üzerine büyütülmüş ve bu kürecikler üzerine P3HT'nin bireysel olarak kaplandığı görülmüştür. Cihazların geçirgenliği, CdS matrisine Co atomlarının ilave edilmesiyle yakın kızılötesi bölgede artış gösterirken, buna karşılık gelen bir absorpsiyon azalması gözlemlenmiştir. Fotolüminesans (PL) verileri, PL pik şiddetinde bir düşüş olduğunu ve bu durumun, bant aralığında radyatif olmayan rekombinasyon merkezleri olarak işlev gören ek kusur seviyelerinin oluşumuna işaret ettiğini göstermiştir. Akım yoğunluğu-gerilim (J-V) karakteristikleri, ITO/N719/CdS:Co(5%)/P3HT/Ag cihazının %0,028'lik bir toplam verimlilik elde ettiğini ve bu verimliliğin referans cihazına kıyasla yaklaşık altı kat artış sağladığını göstermiştir. Bu iyileşmenin, CdS:Co/P3HT ara yüzündeki etkin yük ayrımı sayesinde artan elektron-delik çiftlerinin oluşumuna atfedilmektedir.

Anahtar Kelimeler: CdS:Co ince filmler; P3HT; KBÇ; optik özellikler; güç dönüşüm verimliliği

Received: 4/12/2024

Revised: 25/12/2024

Accepted: 3/01/2025

Online Published: 20/06/2025

How to Cite: Yılmaz S., Tomakin M., Bacaksız E. *"A strategy for enhancing the performance of CdS-based hybrid photovoltaic cells via Co addition"* Adana Alparslan Türkeş Science and Technology University Journal of Science, **1** (1): 1-8 (2025).

1. Introduction

In recent years, interest in CdS-based optoelectronic devices has increased due to the advantageous properties of CdS, including its high absorption coefficient, high transmittance, low resistivity, n-type conductivity, and favorable band gap of 2.42 eV at 300 K [1]. These optical and electrical properties make CdS an excellent candidate for applications in photodetectors [2], gas sensors [3], light-emitting diodes (LEDs) [4], and solar cells [5]. In addition to traditional inorganic solar cells, CdS has also been employed as an inorganic component in hybrid solar cells, where it forms a heterostructure with an organic layer. This type of solar cell combines the advantageous properties of both inorganic and organic materials in a single device, leveraging the strengths of each. Specifically, P3HT is commonly employed as the organic layer due to its strong absorption in the visible region, moderate band gap (1.90 eV), good conductivity and hole mobility, flexibility, and compatibility with blends [6].

A good strategy for improving material properties is doping with an appropriate element. For this purpose, Co was chosen due to its abundance and non-toxicity. Previous studies showed that incorporating Co atoms into CdS created additional energy states within the band gap, which enhanced efficiency [7]. Furthermore, Co-doping may lead to more transparent CdS thin films by reducing optical losses [8]. According to our literature review, there is growing interest in studies on CdS-based heterostructures with a focus on photovoltaic characteristics. For instance, Grynko et al. fabricated a CdS/P3HT:PCBM/PEDOT:PSS photovoltaic cell to investigate how variations in CdS nanowire morphology affect photovoltaic performance. They reported a highest power conversion efficiency (PCE=0.027%) for two-layer CdS nanowires [9]. Through spray pyrolysis, Yılmaz et al. fabricated CdS thin films on ITO-coated glass substrates, studying the effect of dye modification on CdS surfaces, achieving an overall efficiency of 0.082% for an N719-modified CdS-based solar cell [10]. While many studies examine the structural, optical, and electrical properties of CdS:Co systems, few investigate the device characteristics of CdS:Co thin films in photovoltaic cells. Our research group previously published the only known study on this topic, where we fabricated a photovoltaic cell with Co atoms in the ITO/CdS/N719/P3HT:PCBM/PEDOT:PSS/Ag configuration and found highest PCE=0.488% for CdS:Co thin films [11]. In this paper, however, we put forward a distinct configuration: the ITO/CdS:Co/N719/P3HT/Ag heterostructure.

In this research, CdS and CdS:Co films were grown by chemical bath deposition (CBD) technique on ITO-coated glass substrates. The contribution of Co-doping to the PCE of ITO/CdS/N719/P3HT/Ag solar cells was studied by varying the Co concentration to 0%, 1%, 5%, and 7%. All the resultant data were analyzed and compared to clarify the involvement of Co atoms in enhancing on the performance of CdS-based hybrid photovoltaics.

2. Methods

CdS and CdS:Co films were synthesized by the CBD onto ITO-covered glass slides. The Co-doping concentrations were set at 0%, 1%, 5%, and 7%. ITO substrates, cut to 1x1.25 cm^2, underwent a cleaning process in an ultrasonic bath, followed by sulfuric acid, distilled water, and ethanol treatments for 10 minutes each. Afterward, all slides were blown using a nitrogen gas flow. The CdS growth solution included 0.02 M $CdCl_2$, 0.05 M CH_4N_2S, 0.05 M NH_4Cl, and NH_4OH dissolved in distilled water, with full preparation details available in our previous paper [11]. The solution was heated up to 75°C on a hot plate and cleaned ITO slides were vertically immersed for 15 minutes to deposit CdS films. For CdS:Co thin films (1%, 5%, and 7% Co), the same procedure was followed, adding 0.02 M $CoCl_2{\cdot}6H_2O$ as a secondary salt. N719 dye was applied to undoped and Co-doped films from a 0.5 mM solution in absolute ethanol using a spin coater at 1000 rpm. P3HT polymer was then coated using a 0.1 g P3HT chlorobenzene solution, also applied at 1000 rpm. Ag paste (area: 0.8×10^{-2} cm^2) was deposited as the front contact, while In metal was used as the back contact. The fabricated devices, designated as Device A (ITO/CdS/N719/P3HT/Ag), Device B (ITO/CdS:Co(1%)/N719/P3HT/Ag), Device C (ITO/CdS:Co(5%)/N719/P3HT/Ag), and Device D (ITO/CdS:Co(7%)/N719/P3HT/Ag), are shown schematically in Fig. 1.

Scanning Electron Microscopy (SEM) (JEOL JSM 6610) instrument was used to examine the morphological characteristics of the devices. Transmittance and absorbance measurements were conducted using a UV–Vis spectrophotometer (SpectraMax M5), which was also used for photoluminescence analysis at an excitation wavelength of 280 nm. The electrical characteristics (J-V) of the fabricated devices were examined with a source meter (Keithley 2410) and a solar simulator (AM 1.5D) operating at a power output of 100 mW /cm^2.

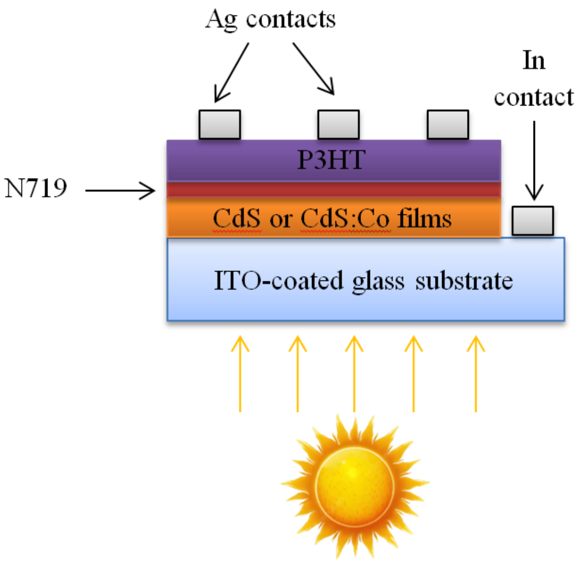

Figure 1. Schematic representation of the fabricated device.

3. Results and Discussion

Figures 2(a)-(d) and (e)-(h) show the surface morphology and cross-sectional images of Devices A, B, C, and D, respectively. In Fig. 2(a), it is observed that the CdS films form spherical structures made up of agglomerated crystallites, with sphere diameters ranging from approximately 0.1 µm to 1 µm, indicating a non-uniform grain size distribution. Notably, each CdS sphere is individually covered by a P3HT layer, rather than being uniformly coated. Device B (Fig. 2(b)) shows a compact, dense, and smooth morphology with reduced grain size, indicating that a low Co-doping concentration (1%) decreases grain size, aligning well with previous reports on CdS:Co films [12]. Some larger grains are also present. Fig. 1(c)-(d) show that Devices C and D have similar surface morphologies, suggesting that increasing the Co concentration up to 7% does not significantly impact grain diameter, shape, or distribution. The microstructure is made up of spherical grains without cracks or pinholes. The individual coverage of P3HT on each CdS sphere remains consistent with Co-doping. Cross-sectional images in Fig. 2(e)-(h) reveal that the thicknesses of Devices A, B, C, and D are approximately 0.52 µm, 0.59 µm, 0.36 µm, and 0.46 µm, respectively.

Figure 3 presents the transmission curves for Devices A, B, C, and D. Device A exhibits low transmittance between 300 and 500 nm, followed by a transmittance range of 5% to 40% from 500 to 650 nm. After 650 nm, Device A's transparency increases, reaching a peak transmittance of 55% at 1000 nm. Conversely, Device B achieves transmittance values above 80% between 650 and 1000 nm, suggesting enhanced transparency likely due to the beneficial effects of Co-doping, consistent with previous reports [13]. Compared to Device A, Device C demonstrates lower transparency, around 70% in the 650-1000 nm range, which may be due to light scattering at grain boundaries because of decreased grain size, which increases boundary lengths [14]. This reduction in transparency might also stem from thickness variations among the devices. Device D shows a transmittance comparable to Device B, exceeding 80%. The absorption edge steepness is often related to the material's crystal quality; thus, Co-doped devices exhibit steeper absorption edges than Device A, indicating Co-doping enhances crystal quality. As indicated by the dashed lines in the figure, an increase in optical transmittance is observed beyond 600 nm for all devices. This behavior confirms that the devices exhibit the characteristic band gap of CdS, which is approximately 2 eV or higher. Additionally, a red shift in the fundamental absorption edge is noted in Devices B, C, and D compared to Device A, suggesting a band gap reduction, likely due to incorporating of Co atoms into CdS host matrix or sp-d exchange interactions between CdS band electrons and the localized d electrons of Co^{2+} ions [15]. An akin band gap diminish was observed in Co-doped CdS nanostructures prepared via spray pyrolysis by Bairy et al. [16]. Overall, Co doping appears to improve the transmittance of devices in the near-infrared (NIR) region.

Figure 4 represents the absorbance data for Devices A, B, C, and D. Device A shows a constant absorbance between 300 nm and 500 nm, followed by a decreasing trend up to 650 nm, corresponding to the band gap of CdS

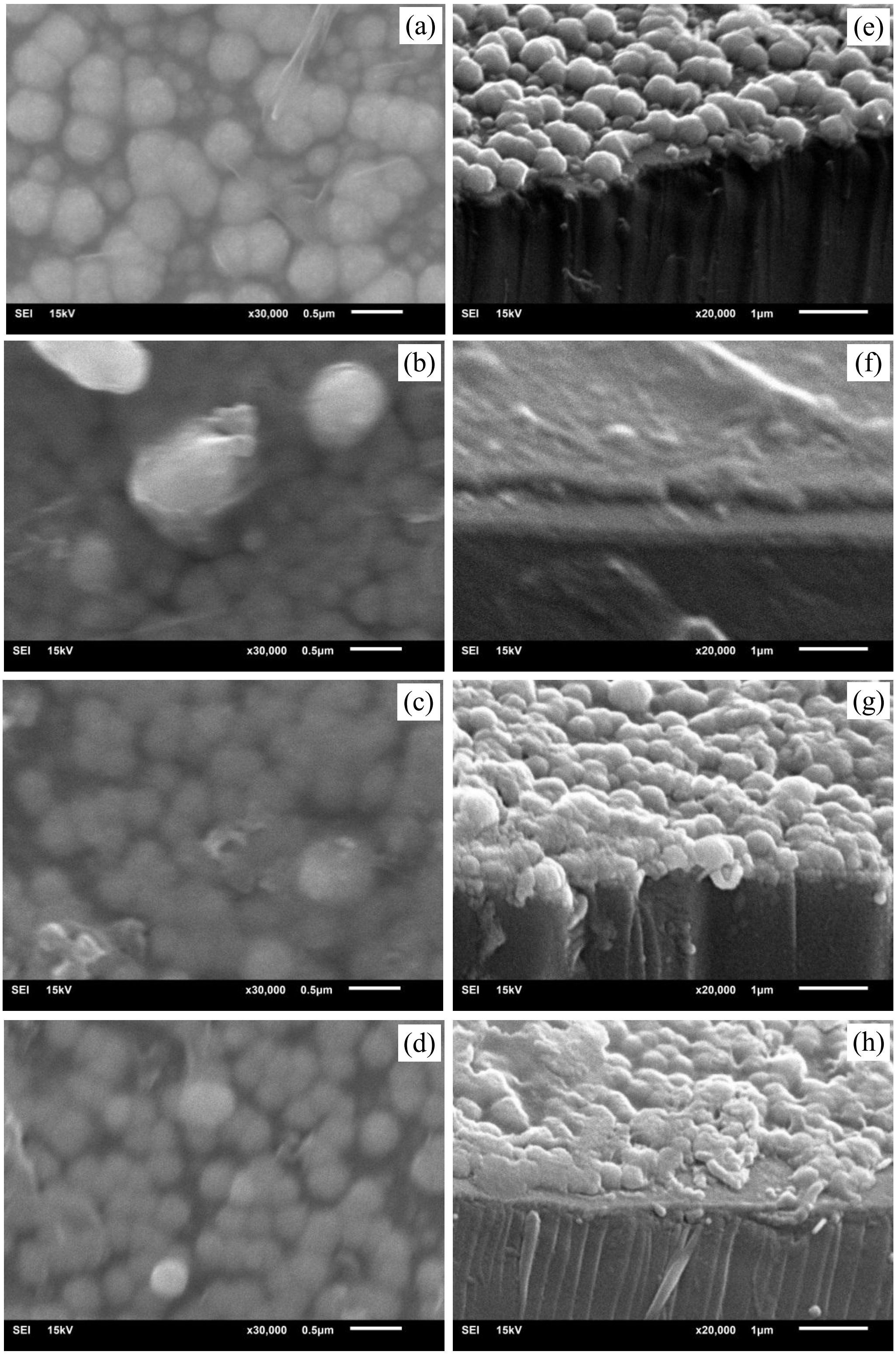

Figure 2. SEM top views of (a) Device A, (b) Device B, (c) Device C, (d) Device D, and cross-sectional views of (e) Device A, (f) Device B, (g) Device C, and (h) Device D.

films. In contrast, Device B exhibits a higher absorption value at 320 nm compared to Device A, but the remainder of the spectrum demonstrates a decreasing trend from 320 nm to 650 nm, remaining lower than that of Device A. Devices C and D display absorption spectra very similar to that of Device B, differing mainly in intensity. Notably, the devices containing Co atoms show lower absorbance than Device A, indicating that the addition of Co atoms to CdS causes a decrement in the absorbance across the spectrum, which aligns with the increased transparency

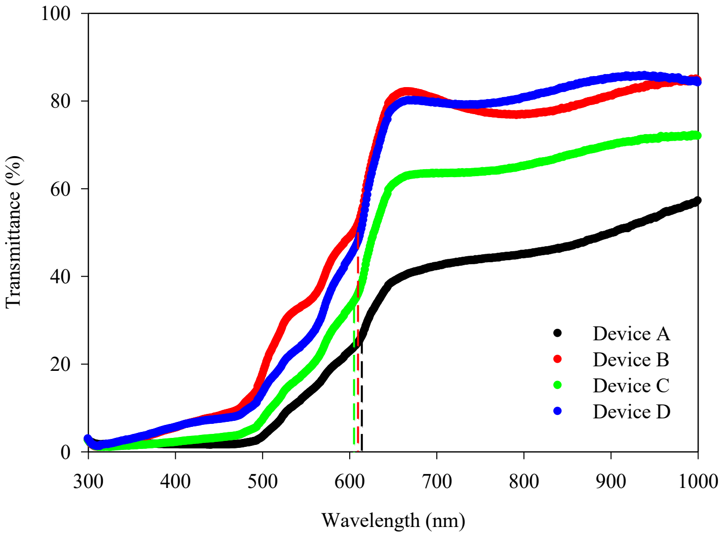

Figure 3. Transmittance data of Device A, Device B, Device C, and Device D.

observed due to Co-doping. This decline in absorption intensity may be attributed to defect states created by the differing sizes of Co^{2+} and Cd^{2+} ions [8]. Deka et al. reported similar findings, noting that the incorporation of Co, Mn, Ni, and Fe atoms decreased the absorbance values of CdS nanocrystals [17]. Conversely, Bairy et al. observed an increment in the absorbance of CdS after Co-doping [16]. Additionally, there appears to be a shift in the fundamental absorption onset of CdS in the devices towards higher wavelengths, which could be associated with a diminish in the band gap, consistent with the findings reported by Maity et al. for CdS:Co quantum dots [18].

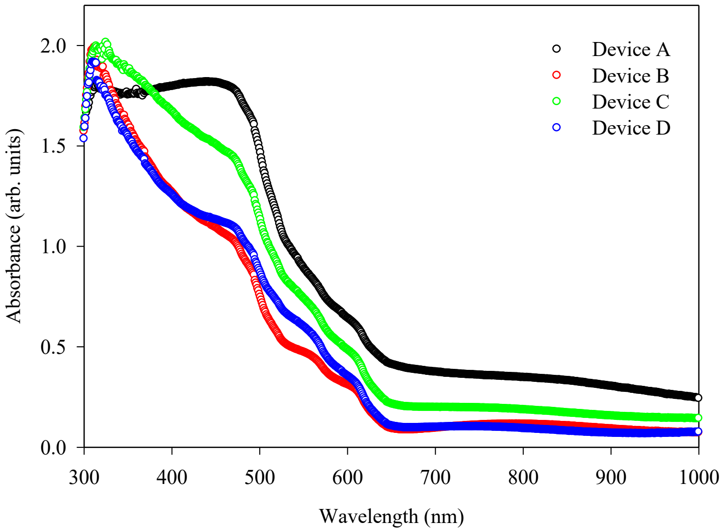

Figure 4. Absorption spectra of Device A, Device B, Device C, and Device D.

Figure 5 demonstrates the photoluminescence (PL) data for Devices A, B, C, D, and the P3HT layer over the range of 300-850 nm. The P3HT layer is observed to dominate the spectra of all the devices in the ranges of 400-500 nm and 600-850 nm, while no peaks corresponding to the 480-600 nm range are detected for the P3HT films. Device A exhibits two distinct peaks at 481 nm and 531 nm. The first peak is referred to radiative transitions occurring between intrinsic defect states and the conduction band, while the second peak could be associated with the band gap of CdS or the Vs defects in the CdS structure [11]. There is no significant change in the peak positions after Co-doping; however, their intensities remarkably decrease, indicating a reduction in the population of these defects. The decrease in PL peak intensity suggests an increase in non-radiative recombination processes, likely due to the formation of additional defect states that act as non-radiative recombination centers. Conversely, the variation in PL peak intensity in the 600-850 nm range indicates exciton dissociation at the CdS/P3HT interface [19]. Device B shows a more intense peak compared to Device A, implying that poorer exciton dissociation occurs between the CdS and P3HT layers. In contrast, Devices C and D demonstrate less intense peaks than Device A, suggesting that efficient exciton dissociation takes place at the CdS/P3HT interface. Therefore, it can be concluded that a higher amount of Co-doping enhances exciton dissociation in the devices, while a lower amount of Co incorporation has a negative effect.

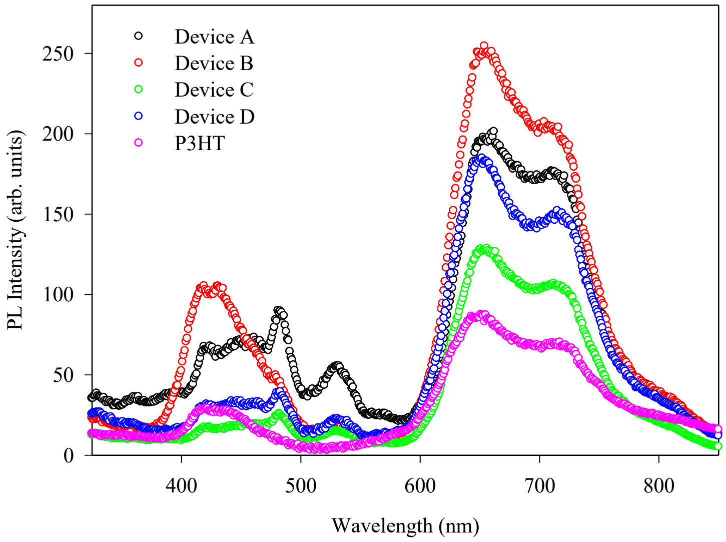

Figure 5. Photoluminescence plots of Device A, Device B, Device C, Device D, and P3HT layer.

Figure 6 presents the J-V characteristics of Device A, Device B, Device C, and Device D, while the solar cell parameters of the devices are summarized in Table 1. Device A shows a short-circuit current density (Jsc) of 0.126 mA/cm^2, an open-circuit voltage (Voc) of 0.115 V, a fill factor (FF) of 0.335, and an overall efficiency of 0.005%. In contrast, the Jsc value for Device B significantly decreases to 0.01 mA/cm^2, although Voc and FF show slight improvements, resulting in an overall PCE of 0.001%. This reduction in efficiency is likely due to poorer exciton dissociation at the CdS:Co/P3HT interface, leading to the formation of fewer e-h pairs, as discussed in the PL analysis. On the other hand, Device C achieves a maximum Jsc of 0.197 mA/cm^2, Voc of 0.371 V, FF of 0.350, and an overall η of 0.028%. This increase in efficiency can be ascribed to the rise in Voc, as listed in Table 1, which suggests effective charge separation between the P3HT and CdS:Co layers, resulting in an increase in e-h pairs. Firoozi et al. reported an increase in Jsc for CdS:Co QDs-sensitized solar cells, attributing it to the occurrence of mid-gap states. Device D exhibits slightly lower values than Device C, showing a modest reduction in overall PCE to 0.019%.

Table 1. Photovoltaic parameters of Device A, Device B, Device C, and Device D.

Device's name	Jsc (mA.cm−2)	Voc (V)	FF	η (%)
Device A	0.126	0.115	0.335	0.005
Device B	0.014	0.156	0.367	0.001
Device C	0.197	0.371	0.350	0.028
Device D	0.169	0.283	0.355	0.019

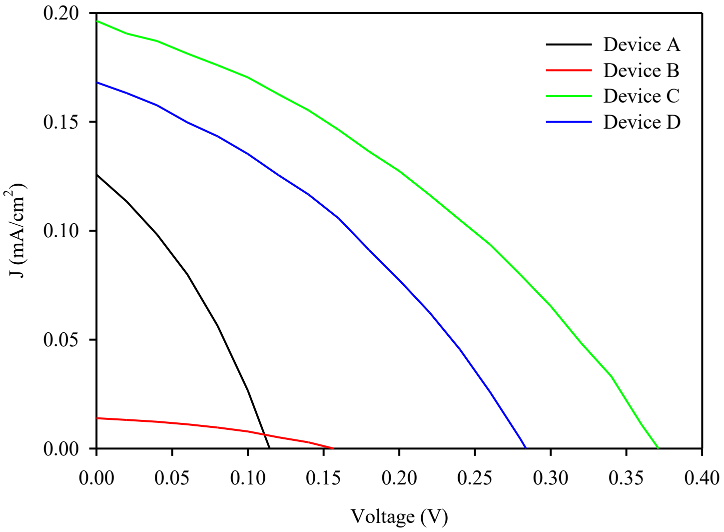

Figure 6. J-V curves of Device A, Device B, Device C, and Device D.

4. Conclusions

This work confirmed the enhancement of PCE in CdS-based hybrid photovoltaics through Co-doping. SEM data indicated that smaller grains were observed for Device B, while Devices C and D exhibited similar surface features to Device A. Devices B and D demonstrated increased transparency in the near-infrared (NIR) region. Photoluminescence (PL) results revealed that Devices C and D had lower PL peaks at higher wavelengths compared to Device A, indicating efficient exciton dissociation occurring between the CdS:Co and P3HT layers. The J-V data showed that a higher concentration of Co-doping caused a significant improvement PCE of the CdS-based photovoltaic cells, with values increasing from 0.005% to 0.028% as the Co concentration rose from 0% to 5%.

Authors' Contributions

SY: Conceptualization, Methodology, Writing - Review & Editing, Validation. **MT:** Data Curation, Writing - Review & Editing. **EB:** Visualization, Investigation, Validation, Writing - Review & Editing, Supervision.

Declaration of Ethical Standards

The author(s) of this article declare that the materials and methods used in this study do not require ethical committee permission and/or legal-special permission.

Conflict of Interest

There is no conflict of interest in this study.

References

[1] Yılmaz, S., Tomakin, M., Polat, İ., Bacaksız, E., (2023). Facile synthesis and characterization of CdS thin flms doped by yttrium atoms, Applied Physics A 129, 579.

[2] Polat, İ., Yılmaz, S., Küçükömeroğlu, T., Tomakin, M., Bacaksız, E., (2024). Performance assessment of oxygenated CdS films-based photodetector, Materials Today Communications 38, 107924.

[3] Vanalakar, S.A., Patil, V.L., Patil, S.M., Deshmukh, S.P., Patil, P.S., Kim, J.H., (2022). Chemical and gas sensing property tuning of cadmium sulfide thin films, Materials Science and Engineering B 282, 115787.

[4] Murai, H., Abe, T., Matsuda, J., Sato, H., Chiba, S., Kashiwaba, Y., (2005). Improvement in the light emission characteristics of CdS:Cu/CdS diodes, Applied Surface Science 244, 351–354.

[5] Rana, M.S., Islam, M.M., Julkarnain, M., (2021). Enhancement in efficiency of CZTS solar cell by using CZTSe BSF layer, Solar Energy 226, 272-287.

[6] Yılmaz, S., Tomakin, M., Ünverdi, A., Aydın, A., Polat, İ., Bacaksız, E., (2020). Structural, morphological, optical analyses of Ni-doped CdS thin films and their photovoltaic performance in hybrid solar cells, Journal of Materials Science: Materials in Electronics 31, 12932–12942.

[7] Han, Y.-X., Yang, C.-L., Sun, Y.-T., Wang, M.-S., Ma, X.-G., (2014). The novel optical properties of CdS caused by concentration of impurity Co, Journal of Alloys and Compounds 585, 503-509.

[8] Pitchaimani, K., Amalraj, L., Muthukumaran, S., (2016). Investigation of structural, photoluminescence and antibacterial behavior of Mn-doped and Co, Mn dual doped CdS thin films by CBD method, Journal of Materials Science: Materials in Electronics 27, 12021–12027.

[9] Grynko, D.O., Fedoryak, O.M., Smertenko, P.S., Ogurtsov, N.A., Pud, A.A., Noskov, Y.V., Dimitriev, O.P., (2013). Application of a CdS nanostructured layer in inverted solar cells, Journal of Physics D: Applied Physics 46, 495114.

[10] Yılmaz, S., Polat, İ., Tomakin. M., Ünverdi, A., Bacaksız, E., (2019). Enhanced efficiency of CdS/P3HT hybrid solar cells via interfacial modification, Turkish Journal of Physics 43, 116 – 125.

[11] Yılmaz, S., Doğan, V., Tomakin, M., Töreli, S.B., Polat, İ., Bacaksız, E., (2024). Introduction of Co atoms into CdS thin films for improving photovoltaic properties, Materials Today Communications 39, 108805.

[12] Kumar, S., Sharma, P., Sharma, V., (2014). Redshift in Absorption Edge of $Cd_{1-x}Co_xS$ Nanofilms, IEEE Transactions on Nanotechnology 13, 343-348.

[13] Sharma, B., Lalwani, R., Das, R., (2023). Spectroscopic Studies of CdS Nanocrystalline Thin Films Synthesized by Sol–Gel Spin Coating Technique for Optoelectronic Application: Influence of Co-Doping, Brazilian Journal of Physics 53, 42.

[14] Saravanakumar, S., Chandramohan, R., Premarani, R., Devadasan, J.J., Thirumalai, J., (2017). Studies on Dilute Magnetic Semiconducting Co-Doped CdS Thin Films Prepared by Chemical Bath Deposition method, Journal of Materials Science: Materials in Electronics 28, 12092–12099.

[15] Giribabu, G., Murali, G., Reddy, D.A., Liu, C., Vijayalakshmi, R.P., (2013). Structural, optical and magnetic properties of Co doped CdS nanoparticles, Journal of Alloys and Compounds 581, 363-368.

[16] Bairy, R., Kulkarni, S.D., Murari, M.S., Narasimhamurthy, K.N., (2020). An investigation of third-order nonlinear optical and limiting properties of spray pyrolysis-deposited Co:CdS nanostructures for optoelectronics, Applied Physics A 126, 380.

[17] Deka, K., Kalita, M.P.C., (2018). Structural phase controlled transition metal (Fe, Co, Ni, Mn) doping in CdS nanocrystals and their optical, magnetic and photocatalytic properties, Journal of Alloys and Compounds 757, 209-220.

[18] Maity, P., Singh, S.V., Biring, S., Pal, B.N., Ghosh, A.K., (2019). Selective near-infrared (NIR) photodetectors fabricated with colloidal CdS:Co quantum dots, Journal of Materials Chemistry C 7, 7725-7733.

[19] Zhong, M., Yang, D., Zhang, J., Shi, J., Wang, X., Li, C., (2012). Improving the performance of CdS/P3HT hybrid inverted solar cells by interfacial modification, Solar Energy Materials and Solar Cells 96, 160-165.

[20] Firoozi, N., Dehghani, H., Afrooz, M., (2015). Cobalt-doped cadmium sulfide nanoparticles as efficient strategy to enhance performance of quantum dot sensitized solar cells, Journal of Power Sources 278, 98-103.